Journal of Applied Fluid Mechanics, Vol. 17, No. 4, pp. 912-925, 2024.
Available online at www.jafmonline.net, ISSN 1735-3572, EISSN 1735-3645.
https://doi.org/10.47176/jafm.17.4.2018

Investigation of the Flow-Induced Noise and Optimization Design of a Short Tube Throttle Valve

K. P. Zhang[1], D. Z. Wu[1,2,†], J. Y. Wang[3], Y. X. Song[3], Z. B. Feng[4], Y. C. He[4] and L. H. Xuan[4]

[1] *Institute of Process Equipment, College of Energy Engineering, Zhejiang University, Hangzhou 310027, China*
[2] *The State Key Laboratory of Fluid Power Transmission and Control, Zhejiang University, Hangzhou 310027, China*
[3] *School of Thermal Engineering, Shandong Jianzhu University, Jinan 250101, Shandong, China*
[4] *Zhejiang DunAn Artificial Environmental Equipment Co., Ltd., Zhuji 311835, China*

†Corresponding Author Email: wudazhuan@zju.edu.cn

ABSTRACT

Compared with the globe valves and other on-off valves, cavitation and noise are more severe in the throttle control valve of the refrigerating system due to the higher saturated vapor pressure of the refrigerant. A short tube throttle valve (STTV) is an important throttle control component and cavitation noise easily occurs because of the pressure drop caused by flow throttling. To suppress the cavitation noise, this paper proposed a numerical investigation verified by experimental data into cavitation and noise characteristics inside the STTV. Three kinds of typical throttle valve structures are proposed in this study. The flow field and cavitation noise of the STTV under different refrigerant flow rates were analyzed numerically. The noise levels of the prototype and three optimized structures are comparatively assessed and analyzed. The findings indicate that the level of cavitation noise rises with an increase in flow rate through the STTV. Specifically, when the flow rate transitions from 0.014 kg/s to 0.024 kg/s, there is a corresponding increase in noise levels, moving from 102.8 dB to 122.5 dB. There is less cavitation noise upstream and the flow is stable, while the noise is mainly concentrated downstream with symmetrical distribution characteristics. The distribution seems to have small noise near the internal wall, while large noise is in the center of the downstream in the STTV, and the maximum noise is observed at the corner of the valve seat of the valve outlet. The optimized valve featuring a slope structure on the valve seat significantly reduces cavitation noise, with a maximum noise reduction of 24.94 dB compared to the prototype valve.

Article History

Received June 28, 2023
Revised November 7, 2023
Accepted November 18, 2023
Available online January 30, 2024

Keywords:

Short tube throttle valve
Cavitation
Noise
Phase change
Refrigerating system

1. INTRODUCTION

STTV is predominantly used in air conditioning to manage the phase of refrigerant, thereby facilitating cooling and heating processes within these systems. The principles of throttling and pressure drop in STTV are also implemented by the orifice plate, similarly to how they are applied in traditional capillaries. In fact, there is only liquid refrigerant at the valve inlet, and a gas–liquid two-phase flow exists at the outlet. This is because the throttle valve produces a pressure drop during the throttling process. When the refrigerant flows into the STTV at high pressure, the local pressure in the throttle valve is reduced due to the throttling effect of the valve. When the pressure is below the saturated vapor pressure of the refrigerant, issues such as severe cavitation often arise in the throttle valve's flow, resulting in a two–phase flow state at the valve's outlet. (Park et al., 2022; Li et al., 2022). Vibration and noise occur when the local pressure is higher than the saturated vapor pressure of the refrigerant (Valdés et al., 2014; Zhang et al., 2020). Consequently, cavitation inception and collapse are the main reasons for STTV noise.

Numerous pertinent studies have been conducted due to the detrimental impacts of cavitation and noise in throttle valves (Kim & O'Neal 1994; Yang & Zhang, 2005; Zhang & Yang, 2005; Valdés et al. 2014; Xu et al., 2016; Liu et al., 2017, 2019). The intensity of cavitation and flow noise of the throttle valve is related to many factors, such as the structure and number of valves, the state parameters of the inlet and outlet, and the shape and flow rate of the fluid. Zhao et al. (2022) found that the number of throttling windows, pressure difference, valve opening and flow direction of the sleeve regulating valve would have an impact on cavitation. Liu et al. (2022) utilized a visualization system with high–speed to investigate the intention and evolution of cavitation in the internal flow channel of an injector ball

NOMENCLATURE

ρ	flow density	ρ_k , ρ_ε	the turbulent Prandtl numbers for k and ε respectively
k	turbulence kinetic energy	S_k , S_ε	user-defined source terms
x_i , x_j	pressure coefficient	$C_{1\varepsilon}$, $C_{2\varepsilon}$, $C_{3\varepsilon}$	constants
u_i	velocity of x_i	α	vapor volume fraction
μ	coefficient of viscosity	ρ_v	vapor density
ε	turbulent dissipation rate	$\vec{V}_v$	vapor phase velocity
G_k	the generation of turbulence kinetic energy due to the mean velocity gradients	R_e	vapor generation rate
G_b	the generation of turbulence kinetic energy due to buoyancy	R_c	vapor condensation rate
Y_M	the contribution of the fluctuating dilatation in compressible turbulence to the overall dissipation rate	$\Re_B$	bubble radius
n	bubble number densities	P	liquid pressure
P_v	the saturated vapor pressure at that state	F_{vap} , F_{cond}	evaporation and condensation correction factors
ρ_v , ρ_l	vapor density and liquid density	P_A	sound power
U	turbulent velocity	l	turbulent characteristic length
α_0	sound velocity		

valve. The internal flow field is obtained through numerical simulation with dynamic boundary conditions, and the formation mechanism and nephogram in the cavitation flow of the valve are investigated. The consequences reveal that cavitation initially occurs in the clearance of the ball valve, followed by the deflector hole and exit control hole. The primary cause of cavitation is the low–pressure area created by throttling. Additionally, streamlines and vortices significantly impact the distribution of cavitation. Wang et al. (2022) conducted a comprehensive investigation into the flow and cavity characteristics of tandem multistage pressure–reducing valves, utilizing both experimental and numerical simulation methods in their analysis. It is found that increasing the flow angle is beneficial for increasing the flow coefficient. The cavitation intensity achieves the minimum value when the rake angle of the flow channel is 60% and the flow chamfer is less than 6mm. Wang et al. (2022) analyzed the flow cavitation phenomenon of the control valve in the pipeline through numerical simulation and found that the structure of the control valve at the throttling stage had a significant influence on the cavitation intensity. Habibnejad et al. (2022) investigated the influence of globe valve opening and inlet flow rate on cavitation intensity and found that the cavitation intensity increases significantly with increasing inlet velocity and decreasing opening. Yuan et al. (2019) studied the cavitation–vortex interaction of the internal jet flow in the poppet-valve. Cavitation continues to exist in the core of the vortex, indicating that cavitation has a strong correlation with vortex dynamics. Ye et al. (2019) found that cavitation was an important factor affecting the efficiency of the micropump through numerical simulation. It has been suggested that enhancing the number of inlet valves can effectively mitigate cavitation, enhance pump flow, and consequently, improve pump efficiency. Yang et al. (2019) proposed deploying continuous micro jets around each nozzle injection flow of the baffle–nozzle pilot valve to restrain cavitation. Liang et al. (2016) conducted a numerical analysis to investigate the relationship between the unsteady cavitation process and inlet pressure fluctuation in a water hydraulic poppet valve with high inlet pressure. The study examined the impact of inlet pressure fluctuation and valve groove on the unsteady cavitation process and flow field. Cavitation can be reduced by the presence of a valve groove. Semrau et al. (2019) investigated the cavitation noise of hydraulic systems through numerical simulation and experiment, and found that reducing discharge pressure can reduce the cavitation noise of the system. Ou et al. (2015) found that cavitation in the flow field decreases to varying degrees with increasing outlet pressure or decreasing the inlet pressure. Zhou et al. (2022) experimentally studied the flow noise characteristics of two–phase refrigerant R410A when it flows through an electronic expansion valve under different flow conditions, and found that a low refrigerant flow rate is helpful reducing the flow noise. Berestovitskiy et al. (2015) provided a basis for selecting the perforating sleeve form of a low noise regulator for the hydraulic system. Zhang et al. (2022) conducted both numerical simulations and experimental research, which revealed that the noise generated by two–phase flow increases with an increase in pressure difference between the inlet and outlet of the electronic expansion valve. To address this issue, they proposed a structure featuring a spiral guide vane downstream, thereby achieving the goal of mitigating flow noise.

Based on the existing literature, numerous significant approaches have been proposed to investigate the flow and noise of the throttle valve, including the examination of the impact of structural parameters on the flow field, the study of flow field visualization, the study of the cavitation phenomenon and the study of the combination of experiments and numerical simulation. All these studies provide effective support for revealing the fluid flow and cavitation phenomena in the throttle valve.

Unfortunately, there is insufficient evidence to demonstrate the impact of structural factors on the flow and noise characteristics of the STTV, which is insufficient to reveal either the turbulence structure or its correlation with noise induced by flow. The analysis of

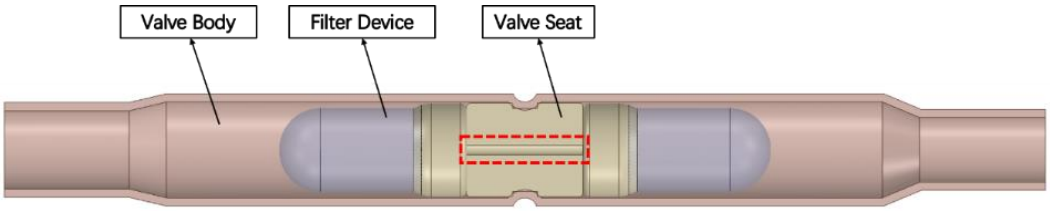

Fig. 1 Three-dimensional geometry of a short tube throttle valve

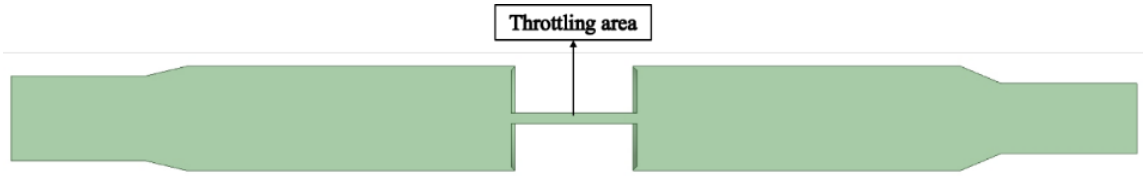

Fig. 2 Short tube throttle valve computational fluid domain

cavitation flow in valves has mainly focused on velocity and pressure in previous studies. Consequently, the mechanism between flow and noise in STTV is not yet adequate.

In this paper, the flow-induced noise of a short-tube throttle valve under different inlet flow rates is analyzed by means of numerical analysis and experimental methods. The flow-induced noise varies with the refrigerant flow rate. Based on the results of numerical analysis, three optimization schemes of the valve body structure of the STTV were proposed, and the flow-induced noise characteristics of the prototype and the optimized models were compared. The optimization model obviously reduced the flow-induced noise. This work aims to serve as a reference for the optimal design of STTV, which holds significant importance in reducing noise during the operation of air conditioning systems.

2. NUMERICAL MODEL AND METHOD

The STTV exhibits remarkable characteristics, including phase transition, vortex generation, and cavitation evolution, due to the pronounced throttling effect resulting from the abrupt contraction and expansion of the flow area. The Reynolds–averaged Navier–Stokes equation (RANS) method is employed, which effectively captures the cavitation process during phase transition due to throttling. In this section, the simplified three–dimensional model of the flow region of STTV was developed. To capture the intricate details of cavitation flow, Fluent software was employed and various models were utilized such as the cavitation model, turbulence model, multi-phase flow model, and noise model for cavitation two-phase flow based on the Reynolds-Averaged Navier Stokes (RANS) method.

2.1 Physical Model

A common STTV for air conditioners is selected in this study. The three–dimensional geometry of the valve is shown in Fig.1. The STTV primarily consists of a valve seat, pipe and filter device. The internal throttling of the STTV is predominantly generated in the region demarcated by the red dashed line in Fig. 1, which corresponds to a throttling orifice passing through the valve seat. To investigate the cavitation and noise issues caused by the short tube throttle, the computational fluid domain is generated through reverse modeling of the aforementioned model, as illustrated in Fig.2.

2.2 Mathematical Modeling

2.2.1 Turbulence Model

The interior of the STTV experiences a significant pressure difference and intricate eddy currents, which could cause the calculation to be unstable and not easily to converge, and the fluids in the STTV are characterized by high Reynolds numbers. The standard k–ε turbulence model, a two–equation turbulent model, is deemed suitable for meeting the simulation requirements. This model also boasts an optimal balance between accuracy and computational efficiency. Consequently, it has been chosen for use in this study.

$$\frac{\partial}{\partial t}(\rho k)+\frac{\partial}{\partial x_i}(\rho k u_i)=\frac{\partial}{\partial x_j}\left[\left(\mu+\frac{\mu_t}{\rho_k}\right)\frac{\partial k}{\partial x_j}\right] +G_k+G_b-\rho\varepsilon-Y_M+S_k \tag{1}$$

$$\frac{\partial}{\partial t}(\rho \varepsilon)+\frac{\partial}{\partial x_i}(\rho \varepsilon u_i)=\frac{\partial}{\partial x_j}\left[\left(\mu+\frac{\mu_t}{\rho_\varepsilon}\right)\frac{\partial \varepsilon}{\partial x_j}\right] +C_{1\varepsilon}\frac{\varepsilon}{k}\left(G_k+C_{3\varepsilon}G_b\right)-C_{2\varepsilon}\rho\frac{\varepsilon^2}{k}+S_\varepsilon \tag{2}$$

where ρ is the flow density, kg/m³ ; k is the turbulence kinetic energy, J ; x_i and x_j are the coordinate positions ; u_i is the velocity of x_i, m/s; μ is the coefficient of viscosity, Pa·s; ε is the turbulent dissipation rate; G_k is the generation of turbulence kinetic energy produced by the mean velocity gradients, J; G_b is the generation of turbulence kinetic energy produced by buoyancy, J; Y_M is the contribution of the fluctuating dilatation in compressible turbulence to the overall dissipation rate; ρ_k and ρ_ε are the turbulent Prandtl numbers for k and ε respectively; S_k and S_ε are user–defined source terms; and $C_{1\varepsilon}$, $C_{2\varepsilon}$ and $C_{3\varepsilon}$ are constants.

The turbulent (or eddy) viscosity μ_t is computed by combining k and ε as follows:

$$\mu_t = \rho C_\mu \frac{k^2}{\varepsilon} \tag{3}$$

where C_μ is a constant.

The model constants $C_{1\varepsilon}, C_{2\varepsilon}, C_\mu, \rho_k$ and ρ_ε are assigned the following default values:

$C_{1\varepsilon}=1.44$, $C_{2\varepsilon}=1.92$, $C_\mu=0.09$, $\rho_k=1.0$, $\rho_\varepsilon=1.3$.

These model constant values are obtained through a large number of experiments and continuous correction, which is proven to be widely used for wall–bounded and free–shear flows with good accuracy and robustness.

2.2.2 Multiphase Flow Model

The Eulerian model, mixture model and VOF (Volume of Fluid) model are commonly used multiphase flow models, and the Eulerian model is mainly used for bubble columns, upwelling and other more complex problems. In consideration of the simplicity of the object of this study, mixture model or VOF model will be selected. Moreover, the mixture model allows interpenetration between phases, which is more suitable for two-phase flow. Consequently, the mixture model is employed to represent the cavitation flow of the STTV.

2.2.3 Cavitation Model

Cavitation is a phenomenon that arises when the static pressure of a fluid falls below its vapor pressure at a specific temperature. Bycomparing the Schnerr–Sauer and Zwart–Gerber–Belamri cavitation models, the Schnerr-Sauer model is used to simulate the cavitation phenomenon, taking into account the phase change process between the gas–liquid phases and the effect of turbulent pressure pulsation on the cavitation pressure. The corresponding mathematical control equations are as follows:

$$\frac{\partial}{\partial t}(\alpha\rho_v)+\nabla\cdot(\alpha\rho_v\vec{V}_v)=R_e-R_c \tag{4}$$

$$\Re_B=\left(\frac{\alpha}{1-\alpha}\frac{3}{4\pi}\frac{1}{n}\right)^{\frac{1}{3}} \tag{5}$$

when $P\leqslant P_v$,

$$R_e=F_{vap}\frac{\rho_v\rho_l}{\rho}\alpha(1-\alpha)\frac{3}{\Re_B}\sqrt{\frac{2}{3}\frac{(P_v-P)}{\rho_l}} \tag{6}$$

when $P\geqslant P_v$,

$$R_c=F_{cond}\frac{\rho_v\rho_l}{\rho}\alpha(1-\alpha)\frac{3}{\Re_B}\sqrt{\frac{2}{3}\frac{(P-P_v)}{\rho_l}} \tag{7}$$

where α is the vapor volume fraction ; ρ_v is the vapor density, kg/m³ ; $\vec{V}_v$ is the vapor phase velocity, m/s; R_e is the vapor generation rate; R_c is the vapor condensation rate; $\Re_B$ is the bubble radius, m; n is the bubble number densities; P is the liquid pressure, Pa; P_v is the saturated vapor pressure at that state, Pa; F_{vap} and F_{cond} are evaporation and condensation correction factors, respectively; and ρ_v and ρ_l are the vapor density and liquid density, respectively, kg/m³.

2.2.4 Noise Model

The broadband noise source model has the characteristic of higher accuracy in the case of more noise sources, and the cavitation noise is mainly distributed in the broadband range. Hence, the broadband noise model (broadband noise sources) is selected for noise analysis, and the control equations are as follows:

$$P_A=\alpha\rho_0\left(\frac{U^3}{l}\right)\frac{U^5}{\alpha_0^5} \tag{8}$$

where P_A is the sound power, W/m³ ; α is the model constant; U is the turbulent velocity, m/s; l is the turbulent characteristic length, m; and α_0 is the sound velocity, m/s.

2.2.5 Mesh and Grid Independency

The STTV structure is relatively straightforward, necessitating the use of a larger grid for mesh generation. Due to the small diameter and area of the throttling region, the grids of this region are locally refined to fulfill the needs of the three-dimensional turbulent model and accurately depict the liquid–vapor interface. Boundary layer grids were generated in the near-wall region, and the range of the $y+$ values on the wall of the flow domain was 10~30. Four distinct mesh models are generated through the use of varying mesh sizes, as depicted in Fig. 3.

To eliminate the impact of grid number on numerical outcomes, the simulation domain's grid count is independently verified. In previous simulation research on cavitation flow, it was found that the parameter of flow rate parameter is significantly influenced by the number of grids in the grid independency test (Jin et al., 2020), Considering the main purpose of this study, the grid independence test is verified when the inlet flow rate is 0.016 kg/s and the outlet pressure is 1 Mpa. The grid independence test results for the outlet flowrate are shown in Table 1.

The table clearly illustrates that the number of grids is directly proportional to the calculation result. The more grids there are, the smaller the deviation is, and the deviation of the outlet flow rate is within 0.1% when the grid number is 540,000. In consideration of the smaller total number of grids, the calculation grid of 540,000 is selected to ensure the calculation accuracy and it will not take long to compute.

2.2.6 Boundary Conditions and Initial Conditions

The R134a refrigerant is used as the medium for calculation. Two monitoring points were selected as the condition of convergence which are marked by the red points in Fig.4.

To investigate the influence of varying inlet flow rates on two-phase flow and noise, boundary conditions were applied to study flow–induced noise in the throttling region of a STTV under diverse flow conditions.

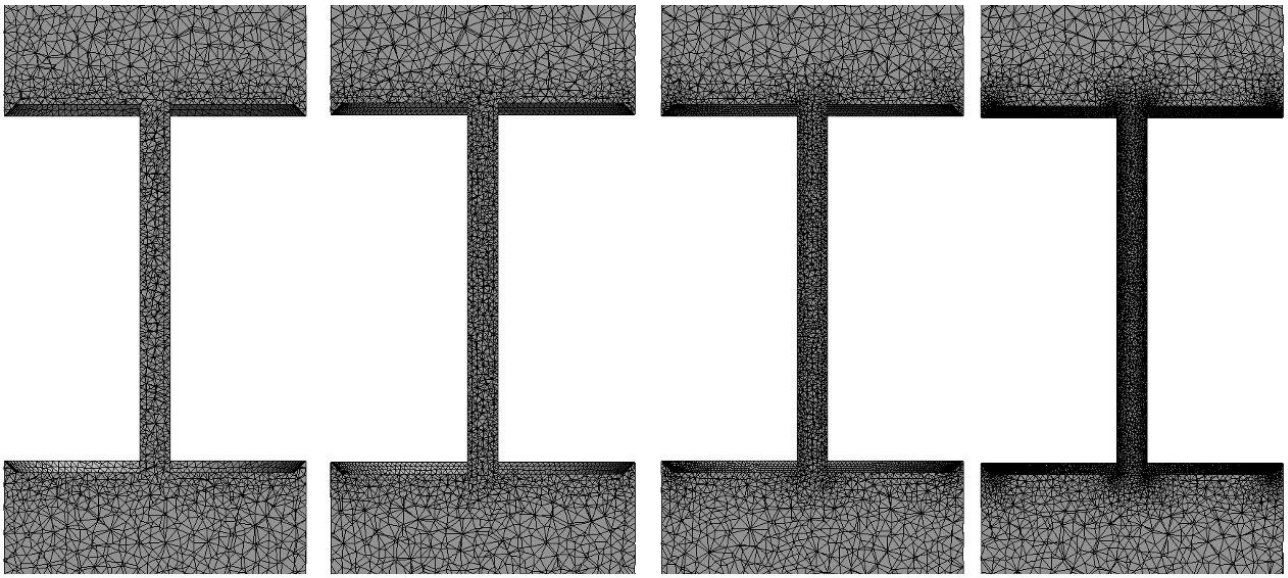

Fig. 3 Grid number comparison chart

Table 1 Grid independence verification

Grid scheme	Grid number/10^4	Inlet /kg/s	Outlet /kg/s	Deviation / %
1	39	0.016	0.01527	4.56
2	43	0.016	0.01555	2.81
3	49	0.016	0.01583	1.06
4	54	0.016	0.01601	0.06

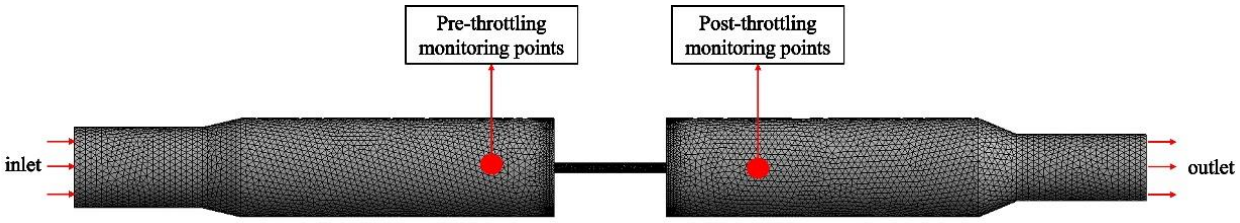

Fig. 4 Schematic diagram of the monitoring points

Specifically, the outlet static pressure was maintained at 1 Mpa, while the mass flow rate inlet was varied from 0.014 kg/s to 0.024 kg/s at intervals of 0.02 kg/s.

3. RESULTS AND DISCUSSION

The unsteady two-phase flow inside the STTV was investigated by numerical methodology in this section. The flow field and cavitation distribution were obtained. Furthermore, the acoustic power level distribution of cavitation with different flow rates was analyzed.

3.1 Analysis of Simulation Results

3.1.1 Analysis of the Pressure Field and Velocity Field

The distributions of flow field pressure and velocity are shown in Fig. 6 and Fig. 7, respectively, for various flow rates (0.014 to 0.024 kg/s) and an outlet pressure of 1MPa. The refrigerant flowed through the STTV with a higher pressure at the inlet and a lower pressure at the outlet throttles based on the principle of the throttle orifice plate. It can be observed from Fig. 6, which the pressure is higher at the inlet and gradually decreases after throttling because of the energy transforming from pressure potential energy to kinetic energy and the pressure at the outlet is almost 1 Mpa. It could also be obtained that there is a higher pressure drop at the throttle orifice with a larger inlet flow rate and a lower pressure drop with a smaller inlet flow rate. In other words, the flow rate can influence the pressure distribution within the valve's flow field. This phenomenon arises due to the larger inlet flow rate possessing greater potential energy. The larger flow rate would have a larger pressure drop if it kept the outlet pressure constant. When the pressure changes, the refrigerant may be accompanied by cavitation. At this point, a temperature change will occur at the orifice. However, because temperature changes only occur in the local area of the orifice, the impact on noise is not significant, so this article will not elaborate separately.

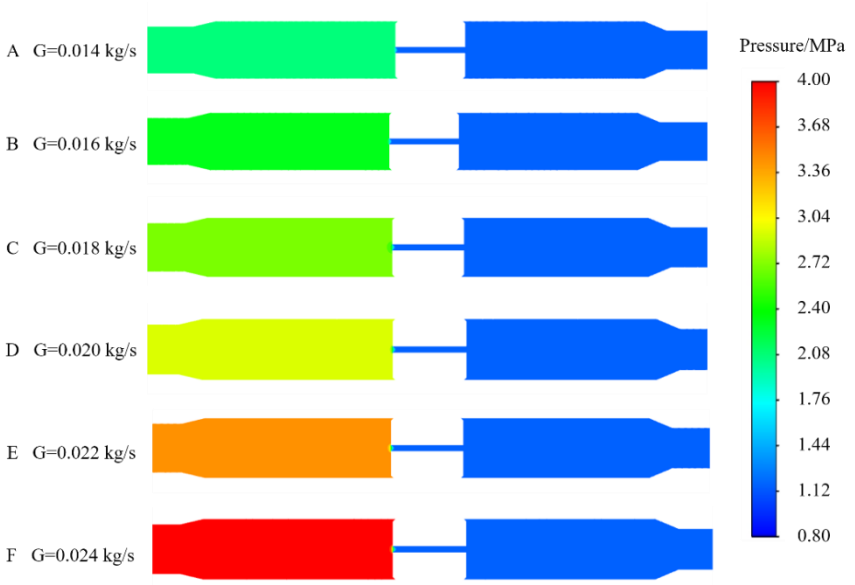

Fig. 5 Pressure field under different inlet flow rates

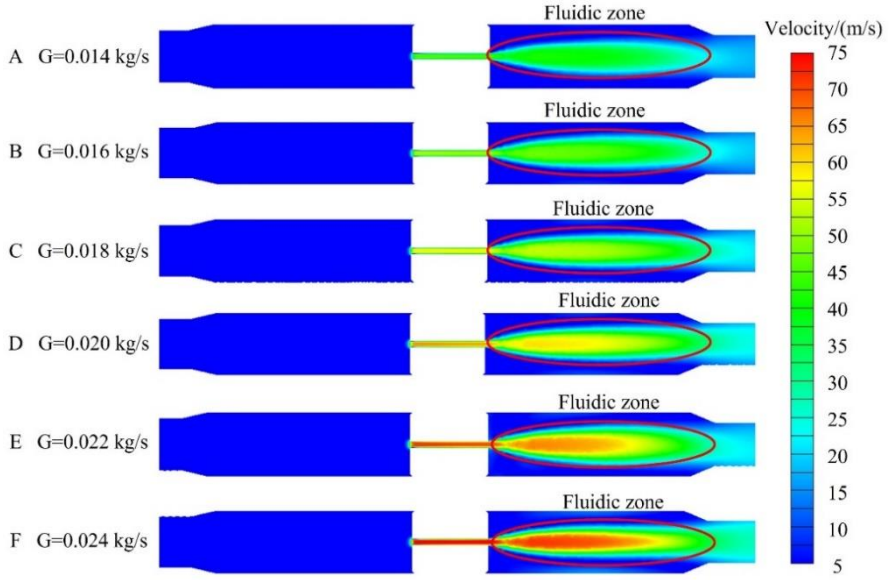

Fig. 6 Velocity field n under different flow rates

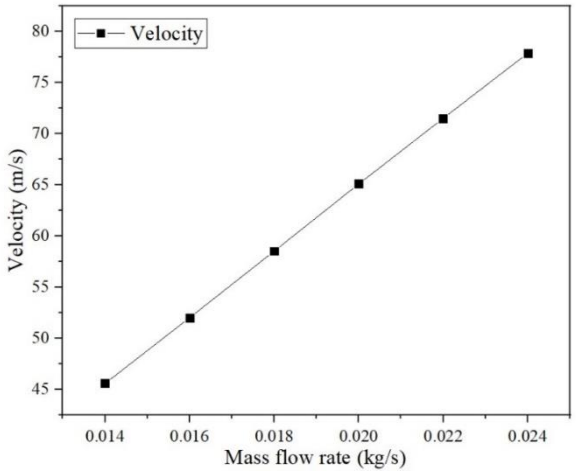

Fig. 7 Maximum flow rate under different flow rates

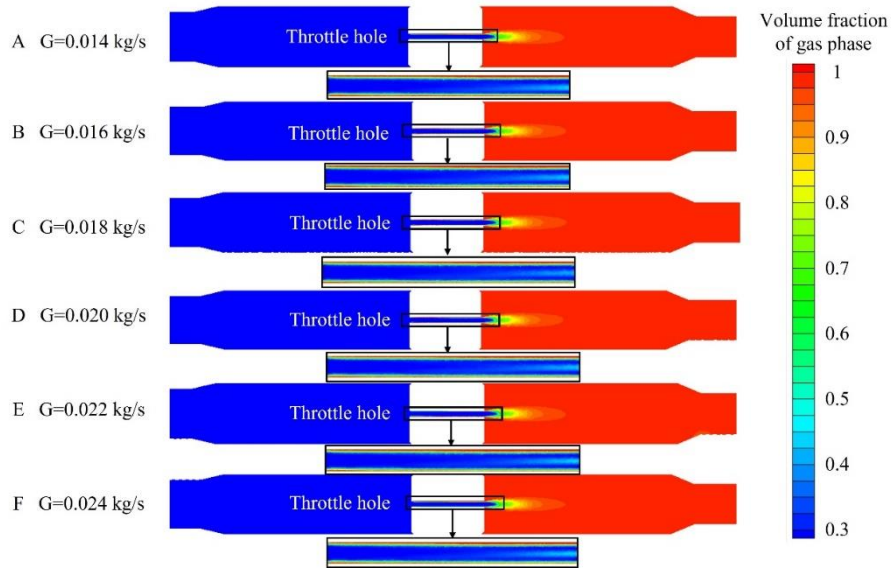

Fig. 8 Gas-phase volume fraction distribution under different flow rates

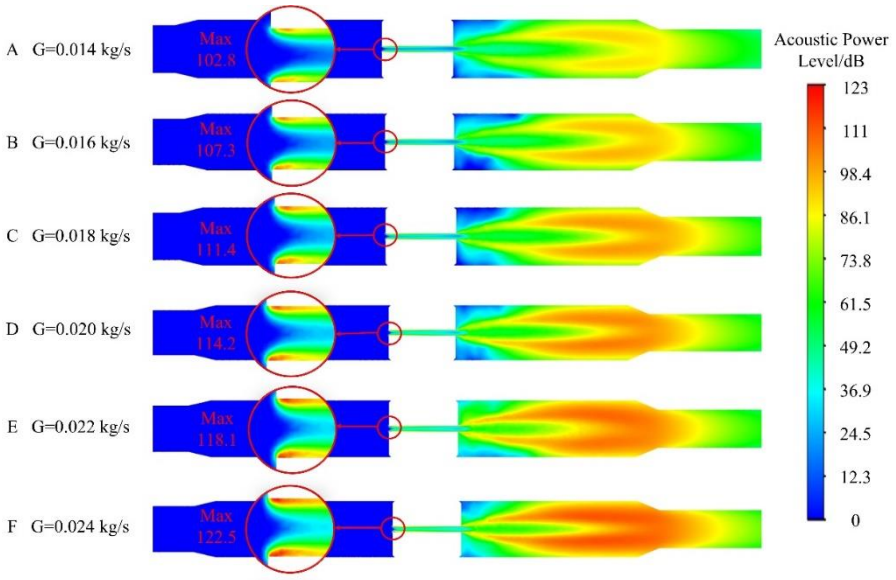

Fig. 9 Acoustic power level distribution under different flow rates

3.1.2 Analysis of the Velocity Field

The refrigerant flows through the STTV at a certain flow rate near the throttle orifice, where the flow velocity increases sharply due to the reduction in the contraction section area. It can be observed from the velocity field presented in Fig. 7 that the maximum flow velocity within the flow field gradually increases with an increase in flow rate. The velocities upstream and downstream near the outlet of the valve are relatively low, and their velocity gradients can be almost entirely disregarded. However, the velocity and the velocity gradient at the throttle orifice are larger due to the pressure potential energy transforming into kinetic energy, which is accompanied by a high velocity, and there is a form of jet with a velocity gradient after the orifice outlet due to the sudden expansion of the tube diameter variation. As depicted in Fig. 8, the maximum flow velocity varies under varying flow rates. A noticeable trend is observed where the highest velocity occurs in the throttle area and progressively rises with an increase in the inlet flow rate. The velocity in the center of the throttle hole is larger, and the velocity in the area near the wall is lower, so a larger velocity gradient is formed.

3.1.3 Gas Phase Volume Fraction Distribution

The refrigerant flows into the short pipe throttle valve in the liquid state, and flows out in gas–liquid two–phase state with throttling and pressure reduction. The gas phase volume fraction distribution of the flow field under varying inlet flow rates is depicted in Fig. 9. From the figure, it is evident that the gas phase volume fraction remains approximately constant despite varying valve flow rates. This can be attributed to the fact that the valve outlet pressure is less than the saturated vapor pressure of the refrigerant, leading to a pronounced downstream cavitation phenomenon. Although the level of cavitation in the flow field is not the same at different flow rates, the distribution states are extremely similar. The gas phase volume is gathered at the downstream area of the valve under different flow rates, which are

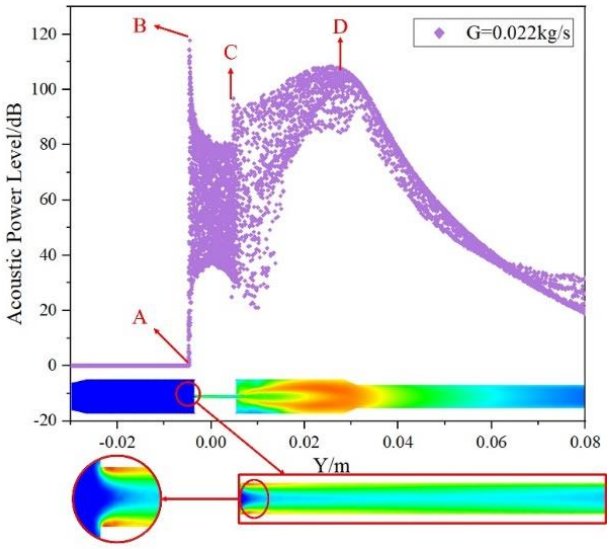

Fig. 10 Acoustic distribution along the Y direction on the XY section with G=0.022 kg/s

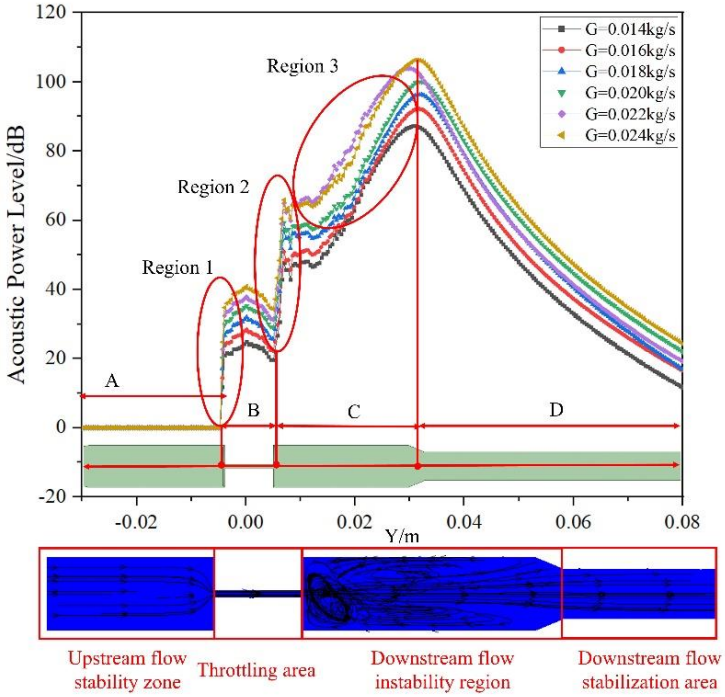

Fig. 11 Noise distribution and trace diagram along the Y direction under different flow rates

distributed symmetrically. It can also be clearly seen near the throttle hole area of the valve that cavitation is generated along the wall, and there is no accumulation of cavitation at the center, due to the high-velocity flow in this area. However, the downstream flow rate is smaller, and the pressure at the outlet of the valve is lower than the saturated pressure, so the cavitation accumulates downstream, and the cavitation phenomenon is significant.

3.1.4 Acoustic Power Level Distribution

The flow of refrigerant is often accompanied by the generation of noise. Part of the noise is generated by fluid dynamic noise, which results from the collision between fluids and the wall during the fluid flow process; the other part is the two-phase flow generated by fluid cavitation, and cavity shifts in tandem with the fluid until the pressure surpasses the saturated vapor pressure of the refrigerant. The bubble collapse generates a significant amount of energy, some of which is released as radiation and noise. Figure 10 is the acoustic power lever distribution of the valve under different flow rates. The noise predominantly manifests in the downstream region of the valve, exhibiting a symmetrical pattern. The peak noise level in the flow field is observed near the inlet of the throttle tube, which is demarcated by a red line. As the flow rate increases from 0.014 kg/s to 0.024 kg/s, the maximum noise value of the flow field escalates from 102.8 dB to 122.5 dB. These results reveal that a gradual rise in the noise level within the flow field as the valve inlet flow rate increases. The acoustic distribution along the Y-direction on the XY section is depicted in Fig. 11,

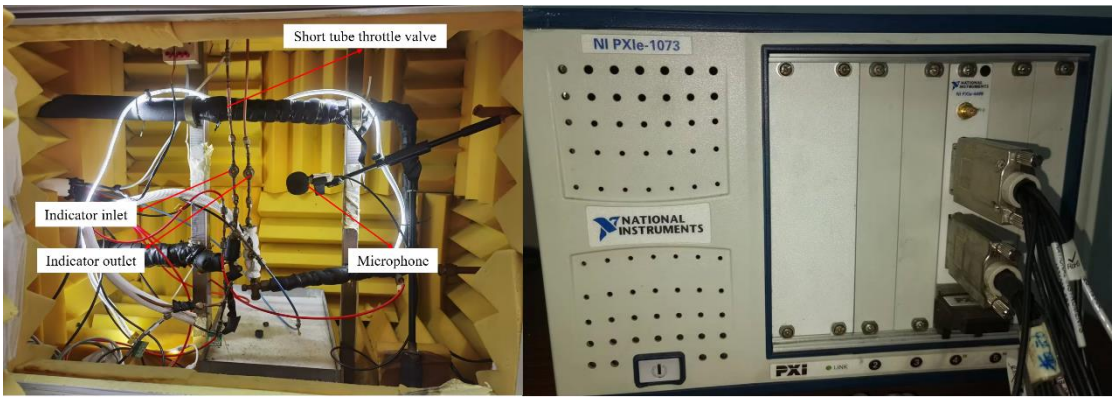

a Noise measurement experimental platform b Data acquisition instrument

Fig. 12 Acquisition experimental platform of acoustic signal

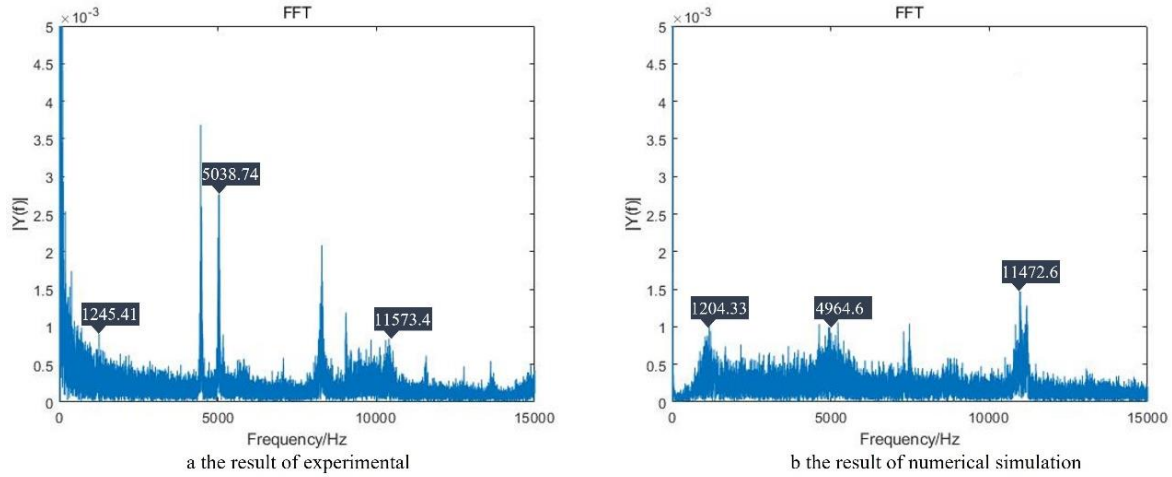

a the result of experimental b the result of numerical simulation

Fig. 13 Results of the experiment and numerical simulation on the acoustic signal

under conditions where G=0.022 kg/s. The noise is approximately 0 before point A at the upstream of the valve. There is a sudden increase at point B, which is produced by the flow instability caused by the change in flow direction at the corner position. In the B-C interval, that is, the throttling section, the noise at this position has been reduced, but there is another extreme value when encountering the corner at point C, which is the exit of the throttling hole. The C–D section is located downstream of the valve, where noise levels increase. However, after point D, the noise begins to decrease.

Figure 12 illustrates the noise distribution and trace diagram along the Y direction under different flow rates. It can be observed from the figure that the noise level in section A is almost zero, as confirmed by the trace diagram of the flow field. This indicates that the flow in this area is relatively stable and there is minimal energy loss. There are three noise extremum value regions in the whole flow process. There is a sudden noise increase in region 1, which is due to the shrinkage of the tube diameter during throttling (as shown in the trace diagram). As the flow velocity increases, the conservation of momentum dictates that a portion of the kinetic energy is converted from pressure potential energy. At the same time, the energy loss is radiated in the form of sound energy, so the phenomenon of a sudden increase in noise occurs. The same phenomenon in which noise suddenly increases occurs in region 2, but for a different reason. The flow rate of the refrigerant flowing out of the orifice is relatively large; when the flow direction changes, it will be subject to greater resistance, the energy loss will be greater, and the radiated sound energy will be greater, which is the reason noises suddenly increases. Section B–C has a slope increase in noise. The trace diagram reveals a highly turbulent flow in this section, with the presence of three distinct vortices. Due to the existence of the vortex, the pressure pulsation in this area is more significant, resulting in an increase in flow-induced noise. In the C–D section, the turbulence phenomenon is obviously weakened, and the noise in this area also tends to decrease.

3.2 Experimental Comparison and Analysis

To validate the accuracy of the numerical analysis，the test is performed through the noise experimental platform under the G=0.016 kg/s condition in this study. As shown in Fig.12, the experimental platform for acoustic signal acquisition was constructed to measure the running noise. The acoustic signal is obtained by the microphone with a sampling rate of 51,200 and a duration of 1 second. The comparison between the experimental and simulated results is conducted under the operating conditions of an outlet pressure of 1 MPa and an inlet flow rate of 0.016 kg/s, as illustrated in Fig. 13. It can be observed from the figure that the frequency

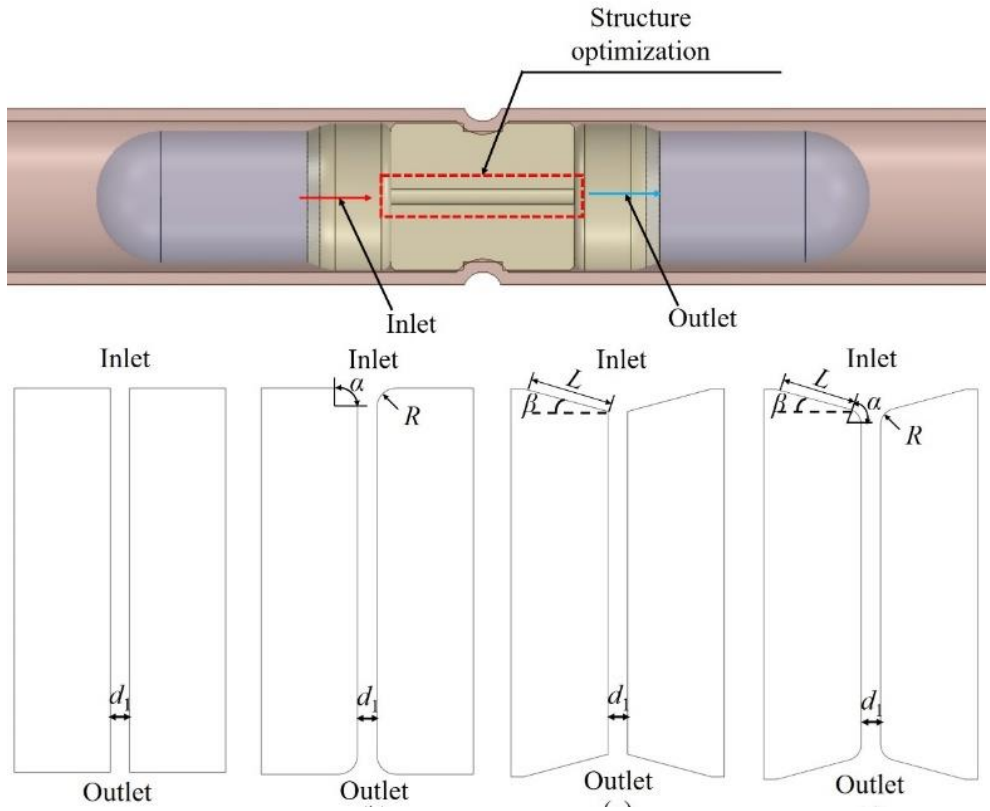

Fig. 14 Sketch of the optimization scheme of the STTV:(a) prototype valve; (b) valve seat with fillet (VS-F); (c) the valve seat with slope(VS-S); (d). Valve seat with fillet and slope(VS-FS)

Table 2 Detailed dimensions of the SSTV

SSTV		Parameters				
		d_1(mm)	α (°)	R (mm)	β (°)	L (mm)
Original		1	-	-	-	-
VS-F		1	90	1	-	-
VS-S		1	-	-	15	2.9
VS-FS		1	75	1.6	15	2.3

spectrum distribution of noise obtained by the experiment ranges from 1245.41 Hz to 11573.4 Hz, while the range from 1204.33 Hz to 11472.6 Hz by numerical calculation. Therefore, the experimental results are consistent with those obtained by numerical calculation, which verifies the reliability of the numerical calculation.

Additionally, some test uncertainties could lead to deviations between test results and simulation values. The purity of the refrigerant will affect the test results, and impurities in the refrigerant will affect the flow and noise of the air conditioning system. The noise insulation of the test chamber is an important factor affecting the test results, and poor sealability of the test chamber can result in data that are not authentic. The accuracy and sensitivity of the test equipment is another factor that affects the test results, and the test results obtained by low frequency and accurate equipment lead to considerable error.

4. STRUCTURE OPTIMIZATION OF THE SHORT TUBE THROTTLE VALVE

4.1 Optimization Scheme

The flow velocity increases with the fluid passing through the throttle orifice due to the contraction of the cross–section, and the flow direction of part of the fluid changes abruptly, which tends to cause flow noise. The structure for the throttling region which could provide a design with a buffer area would be beneficial to solve the noise problem. Fillet and slope instead of a perpendicular scheme is an effective solution.

Based on the above factors, three kinds of optimization schemes of STTV have been proposed to relieve the noise problem in the throttling section of the valve, which are shown in Fig. 14, One consists of an STTV with a 90° fillet on the valve seat (Fig. 14 (b)). The second is a 15° slope on the inlet and outlet of the valve seat (Fig. 14(c)), and the third consists of a 75° fillet

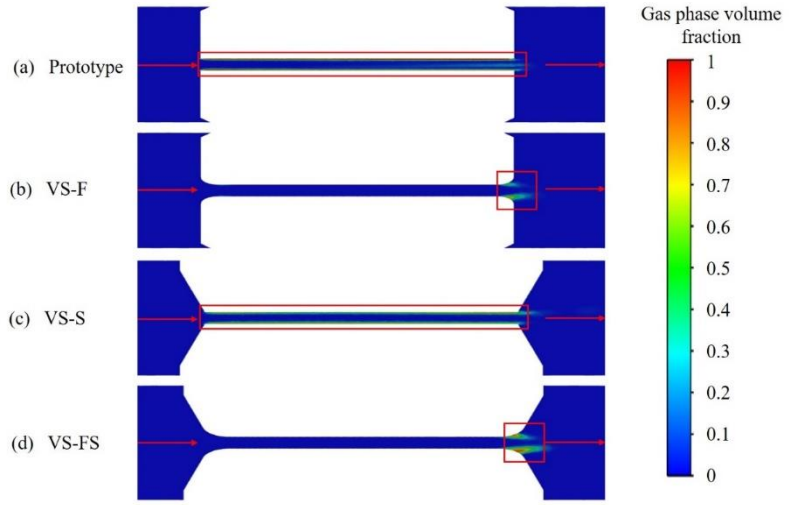

Fig. 15 Comparison of the gas phase volume fraction of the prototype and optimization models

Fig. 16 Acoustic power level distribution of prototype and optimization models

and 15° slope on the inlet and outlet of the valve seat (Fig. 14(d)). The details of the geometric parameters of the three structures are listed in Table 2. The diameters of the throttling hole of these STTVs are the same.

4.2 Comparative Analysis of the Prototype and Optimization Models

To mitigate the noise generated by throttling and cavitation in the flow process of the SSTV. The fillet and slope structure on the throttle region can alleviate the dramatic change in the flow, which would introduce cavitation. Accordingly, the noise induced by the cavitation can be suppressed. Considering an inlet flow rate of 0.016 kg/s and a pressure outlet of 1 Mpa as a case study, this paper compares and analyzes the cavitation and noise of the prototype and the optimization scheme.

4.2.1 Gas Phase Volume Fraction

The volume fraction distribution of the gas phase in the flow throttle section of both the prototype and optimization models is depicted in Fig. 15. The flow direction of the fluid is indicated by the line head in the figure. At the inlet, cavitation is weak and not very obvious, as observed in the figure. However, cavitation is visible in the region of the throttling region, especially at the outlet. Cavitation in the original valve and VS–S valve is generated along the throttle orifice wall, while in the VS–F and VS-FS valves, cavitation is generated along the fillet position of the outlet.

4.2.2 Analysis of the Noise Reduction Effect

In the process of fluid flow, due to the throttling effect and the changing direction of fluid flow, resulting in the noise of fluid colliding with the tube wall and fluid colliding with each other, in addition to the bubble generated at the low–pressure area flowing out with the fluid flow, in the region of higher pressure, it will produce bubble collapse, and thus the role of throttling pressure reduction in the short tube throttling valve, mechanical noise will inevitably occur as well as fluid dynamic noise.

Figure 16 shows the prototype and the optimization models acoustic power level distribution. The noise is predominantly observed in the throttling region and

downstream area of the original model, as evident from the figure. The maximum noise level is observed at the corner of the valve seat outlet, with an acoustic power level of 113.75 dB. Therefore, the model was optimized by changing the valve seat structure. The VS-F model is an optimization scheme that changes the inlet and outlet structure of valve seat from perpendicular to the fillet. Although the maximum noise position is also at the corner of downstream valve seat, the noise has been significantly reduced, from 113.75 dB to 108.70 dB compared with the prototype model, which shows that the noise reduction effect is obvious.

The sudden shrinkage of the tube diameter will also cause noise in the flow. Therefore, the inlet of the valve seat for the gradual reduction and expansion scheme (VS–S) is proposed, to increase the variable-speed buffer area, so that the fluid flows in a gradual manner. The same principle is applied to the outlet, so that the original jet–like flow of fluid along the slope, effectively reduces the flow noise. As shown in Fig. 16(c), the noise position is similar to that of the prototype model, noise reduction is effective by replacing the abruptly reduced valve seat with a gradual reduction surface with a slope, and the maximum acoustic power level is decreased from 113.75 dB in the prototype model to 88.81 dB. The scheme of VS–FS which combines VS–F and VS–S also reduces the acoustic power level, but the noise reduction effect is not obvious, and the maximum acoustic power level is decreased from 113.75 dB in the prototype model to 111.75 dB. The reason why the fillet and slope structure for the inlet and outlet of the throttling orifice could reduce the acoustic power level is that both of these schemes can alleviate the impact of upstream fluid and reduce the extent of sudden shrinkage of the tube diameter. Compared with the three optimization models, the slope structure on the valve seat (VS–S) is the best scheme to reduce the cavitation noise.

5. CONCLUSION

In the current study, the two-phase flow of refrigerant flowing through a short tube throttle valve is numerically simulated and validated for reliability, and the flow rate is a factor affecting the flow–induced noise. Through the optimization of the existing model, three distinct types of low–noise short tube throttle valves have been successfully designed, leading to several significant conclusions:

(1) The noise generated by two–phase flow increases with an increase in the inlet refrigerant flow rate. Specifically, the maximum noise increases from B102.8 dB to 122.5 dB as the flow rate changes from 0.014 kg/s to 0.024 kg/s, provided that the inlet and outlet pressure remain constant.

(2) Three optimization schemes are proposed for the flow characteristics and the location of noise generation: chamfering the valve seat rounding at 90° (VS–F); designing the valve seat with a slope of 15° (VS-S); filleting the corner of valve seat and designing the slope of the valve seat(VS–FS).

(3) There is nearly a small amount of noise upstream. In the prototype model and VS-S model, cavitation occurs mainly at the position of the throttle orifice close to the wall, while in the optimized schemes VS–F model and VS–FS model, cavitation predominantly manifests at the outlet corner of the valve seat.

(4) The optimization schemes under comparison were found to be effective in reducing noise levels when compared to the original model. Specifically, the maximum noise of the flow field was reduced by 5.05, 24.94, and 2.0 dB for VS–FS, VS–S, and VS–FS, respectively. Therefore, the optimization scheme of using an inclined plane structure for the valve seat has the most significant effect on suppressing two-phase flow induced noise.

ACKNOWLEDGEMENTS

This work was supported by the National Natural Science Foundation of China (No. 51839010); the key research and development project of Zhejiang Province, China (No. 2021C03133)

CONFLICT OF INTEREST

The author is responsible for declaring any financial or non-financial interests in this part. If no conflict of interest in there, the author must state that they have no conflicts to disclose.

CREDIT AUTHORSHIP CONTRIBUTION STATEMENT

Kepeng Zhang: Writing – review & editing, Writing – original draft, Software, Methodology, Investigation. **Dazhuan Wu:** Supervision, Methodology, Investigation, Funding Acquisition. **Junyu Wang:** Software, Methodology. **Yongxing Song:** Review &editing, Supervision, Methodology. **Zhongbo Feng:** Supervision, Project administration. **Yuchen He:** Validation, Resources. **Lihua Xuan:** Validation, Resources.

DECLARATION OF COMPETING INTEREST

The authors declare that they have no known competing financial interests or personal relationships that could have appeared to influence the work reported in this paper.

REFERENCES

Berestovitskiy, E. G., Ermilov, M. A., Kizilov, P. I., & Kryuchkov, A. N. (2015). Research of an influence of throttle element perforation on hydrodynamic noise in control valves of hydraulic systems. *Procedia Engineering, 106*, 284-295. https://doi.org/10.1016/j.proeng.2015.06.037

García-Valladares, O., & Santoyo, E. (2014). Modelling of fluid flow through short tube orifices under metastable conditions: A new numerical validation approach for evaluating the mass flow rate with refrigerant mixtures (HFC-407C and HFC-410A). *Applied Thermal Engineering*, *67*(1-2), 520-528. https://doi.org/10.1016/j.applthermaleng.2014.03.056

Habibnejad, D., Akbarzadeh, P., Salavatipour, A., & Gheshmipour V. (2022). Cavitation reduction in the globe valve using oblique perforated cages: A numerical investigation. *Flow Measurement and Instrumentation*, *83*, 102110. https://doi.org/10.1016/j.flowmeasinst.2021.102110

Jin, Z., Qiu, C., Jiang, C., Wu, J., & Qian, J. (2020). Effect of valve core shapes on cavitation flow through a sleeve regulating valve. *Journal of Zhejiang University-SCIENCE A*, *21*, 1-14. https://doi.org/10.1631/jzus.A1900528

Kim, Y., & O"Neal, D. L. (1994). A semi-empirical model of two-phase flow of refrigerant-134a through short tube orifices, Experimental *Thermal and Fluid Science*, *9*(4), 426-435. https://doi.org/10.1016/0894-1777(94)90020-5

Li, G., Ding, X., Wu, Y., Wang, S., Li, D., Yu, W., Wang, X., Zhu, Y., & Guo, Y. (2022). Liquid-vapor two-phase flow in centrifugal pump: Cavitation, mass transfer, and impeller structure optimization, *Vacuum*, *201*, 111102. https://doi.org/10.1016/j.vacuum.2022.111102.

Liang, J., Luo, X., Liu, Y., Li, X., & Shi, T. (2016). A numerical investigation in effects of inlet pressure fluctuations on the flow and cavitation characteristics inside water hydraulic poppet valves. *International Journal of Heat and Mass Transfer*, *103*, 684-700. https://doi.org/10.1016/j.ijheatmasstransfer.2016.07.112

Liu, J., Liu, Z., Wu, J., Li, Z., Chen, P., & Gu, X. (2022). Visualization experiment and numerical calculation of the cavitation evolution inside the injector ball valve. *Fuel*, *329*, 125500. https://doi.org/10.1016/j.fuel.2022.125500

Liu, T., Wang, S., & Xu, Y. (2019). Experimental investigation of stepped short tube orifice as expansion device in domestic air conditioning/heat pump system. *Energy and Buildings*, *193*, 240-249. https://doi.org/10.1016/j.enbuild.2019.04.006

Liu, T., Wang, S., Xu, Y., & Dang, C. (2017). Experimental investigation of mass flow rate difference between forward flow and reverse flow of sub-cooled R-22 through stepped short tube orifices, *Applied Thermal Engineering*, *124*, 1292-1300. https://doi.org/10.1016/j.applthermaleng.2017.06.118

Ou, G. F., Xu, J., Li, W. Z., & Chen, B. (2015). Investigation on cavitation flow in pressure relief valve with high pressure differentials for coal liquefaction. *Procedia Engineering*, *130*, 125-134. https://doi.org/10.1016/j.proeng.2015.12.182

Park, S. H., Phan, T. H., & Park, W.G. (2022). Numerical investigation of laser-induced cavitation bubble dynamics near a rigid surface based on three-dimensional fully compressible model, *International Journal of Heat and Mass Transfer*. *191*, 122853. https://doi.org/10.1016/j.ijheatmasstransfer.2022.122853

Semrau, S., Skoda, R., Wustmann, W., & Habr, K. (2019). Experimental and numerical investigation of noise generation due to acoustic resonance in a cavitating valve. *Journal of Sound and Vibration*, *463*, 114956. https://doi.org/10.1016/j.jsv.2019.114956

Valdés, J. R., Rodríguez, J. M., Monge, R., Peña, J. C., & Pütz, T. (2014). Numerical simulation and experimental validation of the cavitating flow through a ball check valve, *Energy Convers. Manag.* *78*, 776–786. https://doi.org/10.1016/j.enconman.2013.11.038.

Wang, H., Zhu, Z., Xu, H., & Li, J. (2022). Effects of throttling structures on cavitation flow and circumferential uniformity in a control valve. *Engineering Failure Analysis*, *134* ,106025. https://doi.org/10.1016/j.engfailanal.2021.106025

Wang, G., Deng, J., Kou, L., Wang, W., Gao, Q., & Zhu, X. (2022). Study on the influence of structural parameters on the flow and cavitation characteristics of tandem multi-stage pressure-reducing valves. Flow Measurement and Instrumentation, 87,102230. https://doi.org/10.1016/j.flowmeasinst.2022.102230

Xu, Y., He, Q., & Wang, S. (2016). Experimental investigation on pressure drop characteristic of R410A through short tube orifices, *Applied Thermal Engineering*, *109*, 672-677. https://doi.org/10.1016/j.applthermaleng.2016.07.038

Yang, H., Wang, W., Lu, K., & Chen, Z. (2019). Cavitation reduction of a flapper-nozzle pilot valve using continuous microjets. *International Journal of Heat and Mass Transfer*, *133*, 1099-1109. https://doi.org/10.1016/j.ijheatmasstransfer.2019.01.008

Yang, L., & Zhang, C. L. (2005). Two-fluid model of refrigerant two-phase flow through short tube orifice, *International Journal of Refrigeration*, *28*(3), 419-427. https://doi.org/10.1016/j.ijrefrig.2004.06.007

Ye, Y., Chen, J., Pan, Q. S., & Feng, Z. H. (2019). Suppressing the generation of cavitation by increasing the number of inlet check valves in piezoelectric pumps. *Sensors and Actuators A: Physical*, *293*, 56-61. https://doi.org/10.1016/j.sna.2019.04.032

Yuan, C., Song, J., Zhu, L., & Liu, M. (2019). Numerical investigation on cavitating jet inside a poppet valve with special emphasis on cavitation-vortex interaction, *International Journal of Heat and Mass Transfer*, *141*, 1009-1024. https://doi.org/10.1016/j.ijheatmasstransfer.2019.06.105

Zhang, C. L., & Yang, L. (2005). Modeling of supercritical co 2 flow through short tube orifices, *Journal of Fluids Engineering*, 127(6),1194-1198. https://doi.org/10.1115/1.2060738

Zhang, L. H., Wang, J., Song, Y. X., Li, J. J., Wu, D. Z., & Liu, J. T. (2022). Flow-induced noise mechanism and optimization design of electronic expansion

valve. *Vacuum*, *204*, 111335. https://doi.org/10.1016/j.vacuum.2022.111335

Zhang, Y., Xu, J., Cheng, L., Zhao, Y., Peng, S., & Jiang, S. (2020). Exploring cavitation erosion resistance of ZrN nanocrystalline coating prepared by double-cathode glow discharge plasma technique, *Vacuum*, *182*, 109697. https://doi.org/10.1016/j.vacuum.2020.109697.

Zhao, L., Wu, J. Y., Jin, Z. J., & Qian, J. Y. (2022). Cavitation effect on flow resistance of sleeve regulating valve. *Flow Measurement and Instrumentation*, *88*, 102259. https://doi.org/10.1016/j.flowmeasinst.2022.102259

Zhou, S., Zhan, F., & Ding, G. (2022). Experimental investigation on two-phase flow noise characteristics of R410A through electronic expansion valve of multi-split air conditioner. *International Journal of Refrigeration*, *146*, 327-340. https://doi.org/10.1016/j.ijrefrig.2022.11.011